

Article

Phase Transition and Coefficients of Thermal Expansion in $\text{Al}_{2-x}\text{In}_x\text{W}_3\text{O}_{12}$ ($0.2 \leq x \leq 1$)

 Andrés Esteban Cerón Cortés ¹, Anja Dosen ¹, Victoria L. Blair ², Michel B. Johnson ³, Mary Anne White ^{3,4} 
 and Bojan A. Marinkovic ^{1,*} 
¹ Department of Chemical and Materials Engineering, Pontifical Catholic University of Rio de Janeiro (PUC-Rio), Rio de Janeiro 22453-900, Brazil; ceron@aluno.puc-rio.br (A.E.C.C.); adosen@puc-rio.br (A.D.)

² DEVCOM Army Research Laboratory, 6300 Rodman Rd. APG, Adelphi, MD 21005, USA; victoria.l.blair3.civ@mail.mil

³ Clean Technologies Research Institute, Dalhousie University, Halifax, NS B3H 4R2, Canada; michel.johnson@Dal.Ca (M.B.J.); mary.anne.white@dal.ca (M.A.W.)

⁴ Department of Chemistry, Dalhousie University, Halifax, NS B3H 4R2, Canada

* Correspondence: bojan@puc-rio.br; Tel.: +55-21-3527-1954

Abstract: Materials from the $A_2M_3O_{12}$ family are known for their extensive chemical versatility while preserving the polyhedral-corner-shared orthorhombic crystal system, as well as for their consequent unusual thermal expansion, varying from negative and near-zero to slightly positive. The rarest are near-zero thermal expansion materials, which are of paramount importance in thermal shock resistance applications. Ceramic materials with chemistry $\text{Al}_{2-x}\text{In}_x\text{W}_3\text{O}_{12}$ ($x = 0.2\text{--}1.0$) were synthesized using a modified reverse-strike co-precipitation method and prepared into solid specimens using traditional ceramic sintering. The resulting materials were characterized by X-ray powder diffraction (ambient and in situ high temperatures), differential scanning calorimetry and dilatometry to delineate thermal expansion, phase transitions and crystal structures. It was found that the $x = 0.2$ composition had the lowest thermal expansion, $1.88 \times 10^{-6} \text{ K}^{-1}$, which was still higher than the end member $\text{Al}_2\text{W}_3\text{O}_{12}$ for the chemical series. Furthermore, the $\text{AlInW}_3\text{O}_{12}$ was monoclinic phase at room temperature and transformed to the orthorhombic form at ca. $200 \text{ }^\circ\text{C}$, in contrast with previous reports. Interestingly, the $x = 0.2$, $x = 0.4$ and $x = 0.7$ materials did not exhibit the expected orthorhombic-to-monoclinic phase transition as observed for the other compositions, and hence did not follow the expected Vegard-like relationship associated with the electronegativity rule. Overall, compositions within the $\text{Al}_{2-x}\text{In}_x\text{W}_3\text{O}_{12}$ family should not be considered candidates for high thermal shock applications that would require near-zero thermal expansion properties.

Keywords: low thermal expansion; $\text{AlInW}_3\text{O}_{12}$; high-temperature XRPD; dilatometry; DSC



Citation: Cerón Cortés, A.E.; Dosen, A.; Blair, V.L.; Johnson, M.B.; White, M.A.; Marinkovic, B.A. Phase Transition and Coefficients of Thermal Expansion in $\text{Al}_{2-x}\text{In}_x\text{W}_3\text{O}_{12}$ ($0.2 \leq x \leq 1$). *Materials* **2021**, *14*, 4021. <https://doi.org/10.3390/ma14144021>

Academic Editor:
Gianfranco Dell'Agli

Received: 29 June 2021
Accepted: 11 July 2021
Published: 18 July 2021

Publisher's Note: MDPI stays neutral with regard to jurisdictional claims in published maps and institutional affiliations.



Copyright: © 2021 by the authors. Licensee MDPI, Basel, Switzerland. This article is an open access article distributed under the terms and conditions of the Creative Commons Attribution (CC BY) license (<https://creativecommons.org/licenses/by/4.0/>).

1. Introduction

The ceramic phases of the general formula $A_2M_3O_{12}$ and the related families, such as ABM_3O_{12} , ABM_2XO_{12} and $A_2MX_2O_{12}$, have potential for thermal shock resistance applications, since they can present near-zero thermal expansion over wide and technologically relevant temperature intervals, including room temperature (RT) [1]. A potential mechanism for tuning the coefficient of thermal expansion (CTE) in these families is through $A^{3+/4+}$ and $B^{2+/3+}$ cation variation, which leads to changes of rigidity of the framework octahedra [2,3]. More flexible octahedra enhance negative thermal expansion [3].

Based on the knowledge of coefficients of thermal expansion and monoclinic-to-orthorhombic phase transition temperatures in $\text{Al}_2\text{W}_3\text{O}_{12}$ and $\text{In}_2\text{W}_3\text{O}_{12}$ [4–7], the $\text{Al}_{2-x}\text{In}_x\text{W}_3\text{O}_{12}$ system warrants attention. The end member, $\text{Al}_2\text{W}_3\text{O}_{12}$, presents a low positive CTE of $1.51 \times 10^{-6} \text{ K}^{-1}$, as measured by X-ray powder diffraction (XRPD) [5] and $1.17 \times 10^{-6} \text{ K}^{-1}$ from dilatometry [6], as well as monoclinic-to-orthorhombic phase transition temperatures reported at $-6 \text{ }^\circ\text{C}$ [4] and $-22 \text{ }^\circ\text{C}$ [8]. On the other hand, both positive

($3.1 \times 10^{-6} \text{ K}^{-1}$ from XRPD [9]) and negative ($-3.0 \times 10^{-6} \text{ K}^{-1}$ from dilatometry [10]) CTEs were reported for $\text{In}_2\text{W}_3\text{O}_{12}$. The temperature of its monoclinic-to-orthorhombic phase transition was reported to be between 200 °C and 250 °C [4,7,9]. This transition is important because in this family the monoclinic phase exhibits normal positive CTEs, whereas the orthorhombic phase has low or negative CTEs.

Despite the promising properties of the end members, reports on the $\text{Al}_{2-x}\text{In}_x\text{W}_3\text{O}_{12}$ system are scant [11–15]. Evans et al. presented a brief report [11] of dilatometry measurements, showing near-zero to low-positive CTEs for this system in the range of $0.2 \leq x \leq 0.5$, while Mary and Sleight [12], using the same technique, reported zero thermal expansion for the $\text{AlInW}_3\text{O}_{12}$ phase within the temperature range between RT and 727 °C. In a more recent study, Tzvetkov et al. [13] reported a Rietveld XRPD study of $\text{Al}_{1.5}\text{In}_{0.5}\text{W}_3\text{O}_{12}$ and $\text{AlInW}_3\text{O}_{12}$, suggesting both materials were orthorhombic (space group 60, *Pnca*) at RT. In fact, based on visual inspection of XRPD patterns, those authors attributed the orthorhombic structure at RT to all members of the $\text{Al}_{2-x}\text{In}_x\text{W}_3\text{O}_{12}$ system from $x = 0.2$ to 1.4. In a later study [14], the same group reported co-precipitation synthesis of different phases from the $\text{Al}_{2-x}\text{In}_x\text{W}_3\text{O}_{12}$ system, although in contrast with their previous report, the authors stated that the phases for $x \geq 1.3$ were monoclinic at RT.

To the best of the authors' knowledge, there are no thorough non-ambient studies on this system. Furthermore, there is a lack of knowledge on CTE, phase transition and hygroscopicity within the $\text{Al}_{2-x}\text{In}_x\text{W}_3\text{O}_{12}$ system, and there are discrepancies in the literature [13,14] concerning the RT crystal structure of some compositions from this system. In addition, there are no comparative studies of intrinsic (XRPD) and extrinsic (dilatometry) CTE for the $\text{Al}_{2-x}\text{In}_x\text{W}_3\text{O}_{12}$ system, so it is not clear whether this system could be used to achieve near-zero CTE phases; therefore, the evaluation of suitability of the $\text{Al}_{2-x}\text{In}_x\text{W}_3\text{O}_{12}$ ($x = 0.2$ –1.0) system for near-zero thermal expansion materials was the main knowledge gap to be filled by the present study.

Accordingly, the $\text{Al}_{2-x}\text{In}_x\text{W}_3\text{O}_{12}$ system was thoroughly studied using high-temperature XRPD, dilatometry, differential scanning calorimetry and thermogravimetric analysis over the composition range of $0.2 \leq x \leq 1$, and with wide temperature intervals, ranging from cryogenic to high temperatures.

2. Experimental

2.1. Synthesis of $\text{Al}_{2-x}\text{In}_x\text{W}_3\text{O}_{12}$ Powders through Modified Reverse-Strike Co-Precipitation

$\text{Al}(\text{NO}_3)_3 \cdot x\text{H}_2\text{O}$, $\text{In}(\text{NO}_3)_3 \cdot x\text{H}_2\text{O}$ (Alfa Aesar, purity $\geq 99\%$) and $\text{Na}_2\text{WO}_4 \cdot 2\text{H}_2\text{O}$ (Sigma Aldrich, St. Louis, MO, USA, purity $\geq 99\%$) were used as purchased.

Four precursor powders of $\text{Al}_{2-x}\text{In}_x\text{W}_3\text{O}_{12}$ with the nominal chemical compositions $x = 0.2, 0.4, 0.7$ or 1 were prepared using a modified reverse-strike approach [16] through simultaneous dripping of stoichiometric aqueous 0.1 M solutions of $\text{Al}(\text{NO}_3)_3 \cdot x\text{H}_2\text{O}$ and $\text{In}(\text{NO}_3)_3 \cdot x\text{H}_2\text{O}$ into 0.1 M $\text{Na}_2\text{WO}_4 \cdot 2\text{H}_2\text{O}$ with stirring at 600 rpm (Fisam, model 752a) at RT. The pH was not adjusted and naturally tended to a value close to 4 for each mixture (pH = 4.1 for $x = 0.2$, 4.0 for $x = 0.4$, 3.9 for $x = 0.7$, 3.7 for $x = 1$). A white precipitate was instantaneously formed with the addition of nitrates for all chemical compositions. The precipitates were recovered by centrifugation immediately after the formation of precipitates, using an NT 810 centrifuge (Novatecnica, Piracicaba, Brazil) at 4000 rpm, then afterwards were washed three times with anhydrous ethanol (Vetec, 99.9%).

The wet white precipitates were microwave oven dried for 3 min. The dried white precipitate was heated to 600 °C for 1 h and then calcined at 950 °C for 10 h to obtain powders with larger crystallites, which were well suited for XRPD.

2.2. Characterization of $\text{Al}_{2-x}\text{In}_x\text{W}_3\text{O}_{12}$ Powders

To determine intrinsic CTEs and information concerning the possible phase transition from the monoclinic to orthorhombic form, room- and high-temperature X-ray powder diffraction (HT-XRPD) measurements were carried out using a Bruker D8 Advance diffractometer with Cu_α radiation ($\lambda = 1.5418 \text{ \AA}$), with a 2θ scanning step size of 0.01° and

counting time of 2 s per step. High-temperature experiments were performed using a high-temperature Anton-Paar XRK900 camera. HT-XRPD data were acquired at 50, 100, 150, 200, 250, 300, 350 and 400 °C. Intrinsic CTEs (linear and axial) were calculated using the unit-cell parameters (with the standard uncertainties at the fourth decimal place) determined by Le Bail refinement, using Topas-Academic software. The standard deviations for the intrinsic CTE were calculated from the linear fit in the temperature range from room temperature to 400 °C.

Extrinsic CTEs for $\text{Al}_{2-x}\text{In}_x\text{W}_3\text{O}_{12}$ samples in the form of bars were determined using a DIL 402C NETZSCH dilatometer. Green bodies (bars) were prepared using 250 MPa pressing of powders obtained by co-precipitation, mixed with 1 mass% polyethylene glycol and 1 mass% polyvinyl alcohol. Afterwards, green bodies were sintered at 950 °C for 10 h in air. High relative densities (>96% of theoretical density) were obtained for the as-sintered bodies, as measured using the Archimedes method (Supporting Information, Table S1). Dilatometric curves were acquired on sintered bars (diameter 6.5 mm; length 8 mm) on heating from RT to 500 °C at a rate of 5 K min⁻¹ and on cooling at a rate of 3 K min⁻¹. Three measurements were performed for each composition and standard deviations were calculated. The dilatometer had been previously calibrated for CTE measurements using Al_2O_3 standard sample supplied by NETZSCH. CTEs were calculated from heating curves from RT to 500 °C.

Thermogravimetric analyses (TGA) were performed on a Perkin–Elmer STA-6000 simultaneous thermal analyzer. Samples (~20 mg) were heated from RT to 950 °C at 10 K min⁻¹ in synthetic air at a flow rate of 20 mL min⁻¹.

Differential scanning calorimetry (DSC) analyses were conducted in a TA Instruments Q200, equipped with a liquid N₂ cooling head under He purge gas (25 mL min⁻¹), with a heating rate of 20 K min⁻¹ over the temperature ranges from –100 °C to 0 °C and from 0 °C to 300 °C.

3. Results and Discussion

XRPD patterns at RT of four different phases from the $\text{Al}_{2-x}\text{In}_x\text{W}_3\text{O}_{12}$ system ($x = 0.2, 0.4, 0.7$ and 1) are presented in Figure 1. All four powders were single-phased. The unit-cell parameters of $\text{Al}_{2-x}\text{In}_x\text{W}_3\text{O}_{12}$ phases at RT are presented in the Supporting Information, Table S2. Le Bail refinements of the patterns of the $x = 0.2, 0.4$ and 0.7 materials fit very well within the orthorhombic system (space group 60, *Pbcn*); however, the XRPD pattern of $x = 1$ (Figure 1d) was slightly different from the results for the three phases with a lower In³⁺ content. It was very similar to what would be expected for the orthorhombic *Pbcn* space group, but presented additional features, namely two extra diffraction lines situated at 23.8° and 25.9° (2θ), while the most intense peak, close to 22.4° (2θ), was not divided into two separate diffraction lines as it was for orthorhombic system (Figure 1a–c). These features have been attributed in the literature to the monoclinic system (space group 12, *P2₁/a*) [17,18] or *P2₁/n* (space group 14) [8,19]; therefore, the XRPD pattern for $x = 1$ was adjusted to the monoclinic system, which described all experimental diffraction lines very well. As such, the XRPD patterns at RT (Figure 1) suggested that $\text{AlInW}_3\text{O}_{12}$ is monoclinic at RT and not orthorhombic, as previously proposed [13,14].

HT-XRPD patterns of $x = 0.2$ and $x = 1$ phases are depicted in more detail in Figure 2, while complete sets of diffraction patterns up to 400 °C for all phases are available in Supporting Information, Figure S1. Note that the XRPD pattern of the $x = 1$ phase changed to orthorhombic at 250 °C, as evidenced by the disappearance of the two diffraction lines at 23.8° and 25.9° (2θ), as well as the most intense peak, close to 22.4° (2θ), separating into two adjacent diffraction lines.

Proof of In³⁺ incorporation into the orthorhombic crystal structure, in accordance with the nominal chemical compositions of $\text{Al}_{2-x}\text{In}_x\text{W}_3\text{O}_{12}$ ($x = 0.2, 0.4, 0.7$ and 1), is evident from the isothermal plot constructed for 250 °C, which obeys Vegard's law [20] (Figure 3). A near linear unit-cell volume increase with the increase of In³⁺ content (x)

in the orthorhombic $\text{Al}_{2-x}\text{In}_x\text{W}_3\text{O}_{12}$ phase correlates well with the larger radius of In^{3+} (0.80 Å) in comparison to Al^{3+} (0.535 Å) [21].

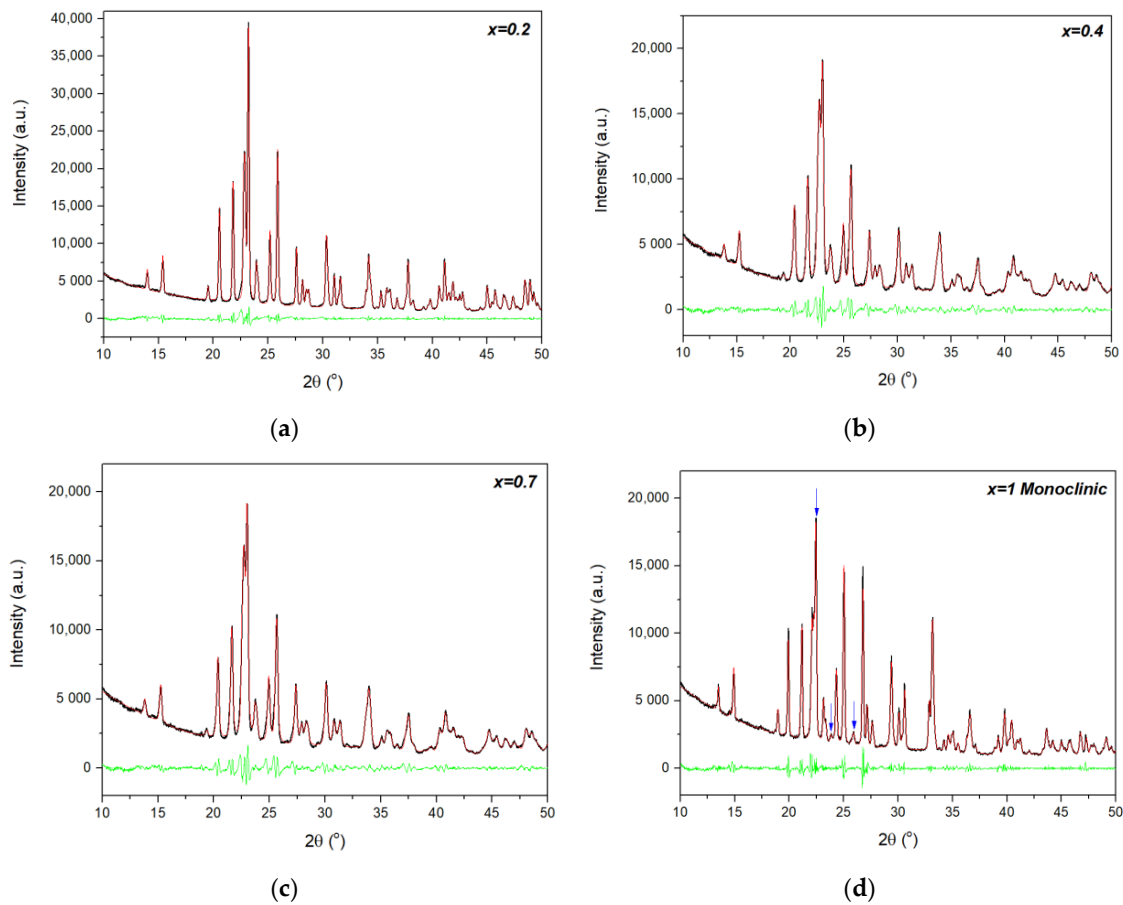
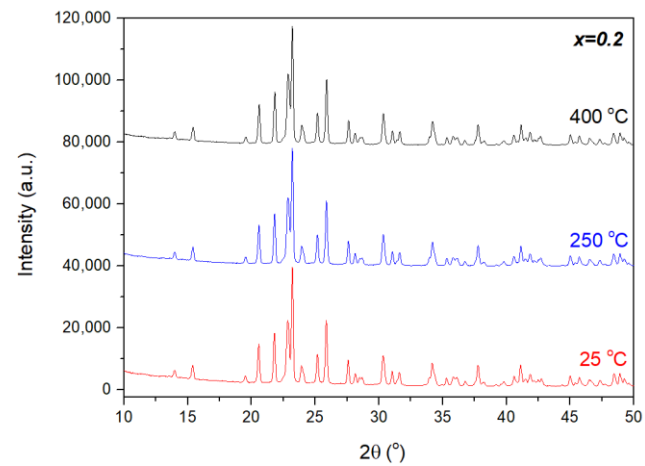
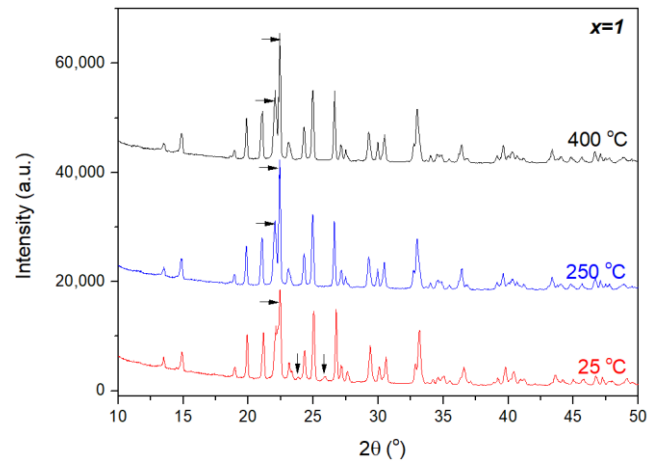


Figure 1. XRPD patterns of $\text{Al}_{2-x}\text{In}_x\text{W}_3\text{O}_{12}$ powders at RT, illustrating Le Bail fits to the orthorhombic $Pbcn$ space group for the compositions (a) $x = 0.2$, (b) 0.4 and (c) 0.7 and to the monoclinic $P2_1/a$ space group for (d) $x = 1$ (to highlight the differences between orthorhombic and monoclinic patterns, the 2θ angle range between 10° and 50° is presented). Experimental profiles are represented by black lines, calculated profiles by red lines and difference profiles by green lines. (d) The arrows show typical diffraction lines for the monoclinic system in the $\text{A}_2\text{M}_3\text{O}_{12}$ family, which are absent in the orthorhombic system.

Table 1 presents linear and axial CTEs for all four $\text{Al}_{2-x}\text{In}_x\text{W}_3\text{O}_{12}$ compositions over the temperature interval between RT and 400 or 500 °C. The plots of natural logarithms of unit-cell parameters (a , b and c) and unit-cell volumes as functions of temperature are available in the Supporting Information, Figure S2. Axial CTEs along the b - and c -axes increased monotonically with increasing x up to $x = 0.7$, while the axial CTE along the a -axis varied up to $x = 0.7$ in a non-monotonical manner. This discrepancy should be verified by higher-resolution synchrotron radiation. Linear CTEs of the $x = 0.2$, 0.4 and 0.7 phases are positive and increase with increasing In^{3+} content (x), appearing more in line with the more positive intrinsic CTE of the end-member $\text{In}_2\text{W}_3\text{O}_{12}$ ($3.1 \times 10^{-6} \text{ K}^{-1}$), as reported by Baiz et al. [9], than the reported negative linear CTE of $\text{In}_2\text{W}_3\text{O}_{12}$ [10]; therefore, the phases in the range between $x = 0.2$ and 0.7 showed a tendency of increased linear CTE in comparison to pure $\text{Al}_2\text{W}_3\text{O}_{12}$. Judging from this behavior, it would not be possible to obtain near-zero CTE at RT and higher within the $\text{Al}_{2-x}\text{In}_x\text{W}_3\text{O}_{12}$ system. The axial CTEs were more positive along the a - and b -axes and negative or low positive along the c -axes. The $x = 1$ phase showed a high linear CTE in the monoclinic form ($\sim 10^{-5} \text{ K}^{-1}$) from RT to 100 °C, in agreement with the literature [22,23], while above 250 °C when orthorhombic it presented a near-zero CTE ($-7.9 \times 10^{-7} \text{ K}^{-1}$).



(a)



(b)

Figure 2. HT-XRPD patterns of $\text{Al}_{2-x}\text{In}_x\text{W}_3\text{O}_{12}$ materials for (a) $x = 0.2$ (orthorhombic) and (b) $x = 1$ (illustrating the phase transition from a monoclinic to orthorhombic structure at 250 °C). (b) The arrows at RT show typical features for the monoclinic system in the $A_2M_3O_{12}$ family, while at higher temperatures the arrows mark separation of the most intense peak into two diffraction lines, which is a feature of an orthorhombic pattern for the $A_2M_3O_{12}$ family.

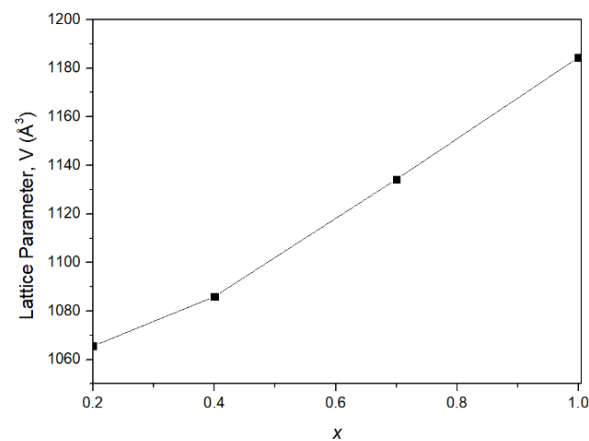


Figure 3. Orthorhombic unit-cell volumes at 250 °C as a function of In^{3+} content (x) in $\text{Al}_{2-x}\text{In}_x\text{W}_3\text{O}_{12}$. Standard deviations are smaller than symbol size.

Table 1. Intrinsic and extrinsic CTEs by axis (α_a , α_b , α_c) and average linear CTE (α_l) in the $\text{Al}_{2-x}\text{In}_x\text{W}_3\text{O}_{12}$ system ($Pbcn$ space group for the orthorhombic phase and $P2_1/a$ for the monoclinic phase) with their standard deviations (standard deviations for $x = 1$ in monoclinic form are one order of magnitude higher than for others, since only three points were considered). Standard deviations for CTEs of the end-members are not reported in the literature [5,9]. Results not referenced to the literature are from the present study. RT refers to room temperature.

x (In^{3+} Content in Chemical Formula)	α_a [K^{-1}]	α_b [K^{-1}]	α_c [K^{-1}]	α_l [K^{-1}]	Temperature Range [$^{\circ}\text{C}$]	Ref.
0	5.94×10^{-6}	-0.994×10^{-6}	-1.31×10^{-6}	1.51×10^{-6}	RT–800 (XRPD)	[5]
0.2	4.98×10^{-6} $\pm 1.3 \times 10^{-7}$	9.47×10^{-7} $\pm 1.3 \times 10^{-7}$	-2.93×10^{-7} $\pm 1.5 \times 10^{-7}$	1.88×10^{-6} $\pm 1.4 \times 10^{-7}$ 4.96×10^{-6} $\pm 1.8 \times 10^{-7}$	RT–400 (XRPD) RT–500 (dilatometry)	-
0.4	3.80×10^{-6} $\pm 2.2 \times 10^{-7}$	2.09×10^{-6} $\pm 2.4 \times 10^{-7}$	8.77×10^{-7} $\pm 2.7 \times 10^{-7}$	2.25×10^{-6} $\pm 2.4 \times 10^{-7}$ 6.29×10^{-6} $\pm 7.0 \times 10^{-7}$	RT–400 (XRPD) RT–500 (dilatometry)	-
0.7	5.52×10^{-6} $\pm 1.2 \times 10^{-7}$	3.92×10^{-6} $\pm 3.2 \times 10^{-7}$	2.22×10^{-6} $\pm 2.3 \times 10^{-7}$	3.88×10^{-6} $\pm 2.2 \times 10^{-7}$ 6.00×10^{-6} $\pm 7.0 \times 10^{-7}$	RT–400 (XRPD) RT–500 (dilatometry)	-
1 ($P2_1/a$)	1.83×10^{-5} $\pm 7.5 \times 10^{-6}$	1.47×10^{-5} $\pm 4.5 \times 10^{-6}$	2.63×10^{-5} $\pm 8.1 \times 10^{-6}$	1.88×10^{-5} $\pm 7.7 \times 10^{-6}$	RT–100 (XRPD)	-
1 ($Pbcn$)	8.47×10^{-7} $\pm 2.9 \times 10^{-7}$	-9.32×10^{-7} $\pm 4.0 \times 10^{-7}$	-2.27×10^{-6} $\pm 4.7 \times 10^{-7}$	-7.87×10^{-7} $\pm 3.9 \times 10^{-7}$ 3.18×10^{-6} $\pm 1.6 \times 10^{-7}$	250–400 (XRPD) 250–500 (dilatometry)	-
2 ($Pbcn$)	-3.1×10^{-6}	11×10^{-6}	1.6×10^{-6}	3.1×10^{-6}	250–600 (XRPD)	[9]

Dilatometric curves for the $x = 0.2, 0.4$ and 0.7 materials (Figure 4a–c) showed positive linear extrinsic CTEs, higher than those measured by XRPD (Table 1). These orthorhombic phases demonstrated the tendency for increased CTE with the increase of In^{3+} content (x), as also observed for the intrinsic linear CTEs. The increased extrinsic CTEs relative to the intrinsic CTEs might be partially understood as a consequence of the anisotropy of elastic constants in the $A_2M_3O_{12}$ family [24]. In addition, dilatometry clearly confirmed the phase transition in $x = 1$ between 150 and 220 $^{\circ}\text{C}$ (Figure 4d), from the denser monoclinic polymorph to the more open (higher volume) orthorhombic form [25].

DSC curves at cryogenic, ambient and above ambient temperatures are presented in Figure 5. Figure 5b shows an endothermic peak (with the onset temperature of ~ 195 $^{\circ}\text{C}$) as another indication of the monoclinic-to-orthorhombic phase transition in the $x = 1$ material. The enthalpy change at the phase transition (2.23 kJ mol^{-1}) is in accordance with the low enthalpy changes usually measured for displacive monoclinic-to-orthorhombic phase transitions in this ceramic family [26], owing to small differences in internal energies and molar volumes between the two phases. The other three DSC curves are practically featureless in the vast temperature range from -100 $^{\circ}\text{C}$ to 300 $^{\circ}\text{C}$. Two faint kinks registered at ~ 130 $^{\circ}\text{C}$ in the DSC curves of $x = 0.4$ and 0.7 materials were likely artefacts, as they were not corroborated either by HT-XRPD or dilatometric measurements.

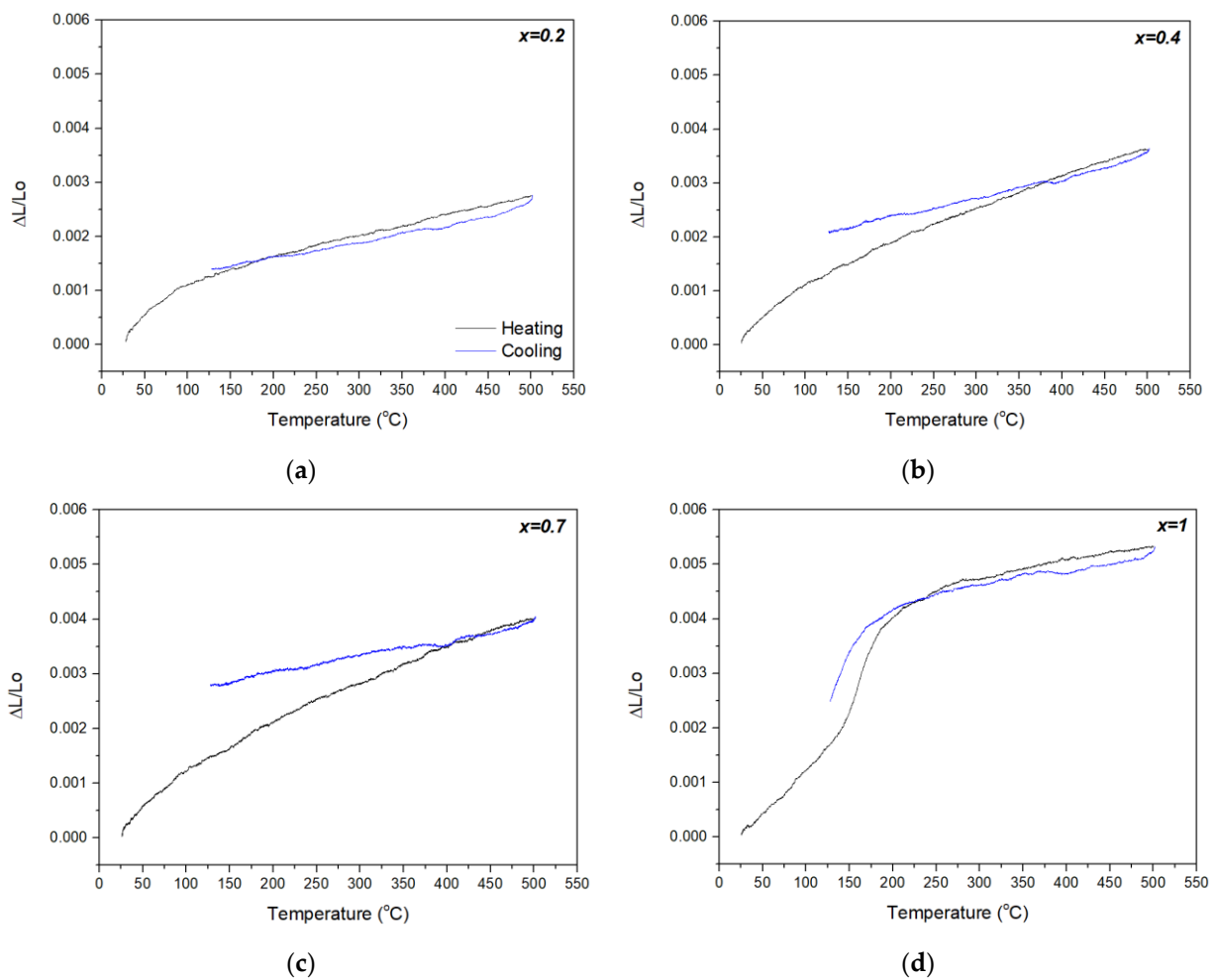


Figure 4. Dilatometric curves of the materials in the family of $\text{Al}_{2-x}\text{In}_x\text{W}_3\text{O}_{12}$: (a) $x = 0.2$; (b) $x = 0.4$; (c) $x = 0.7$; (d) $x = 1$.

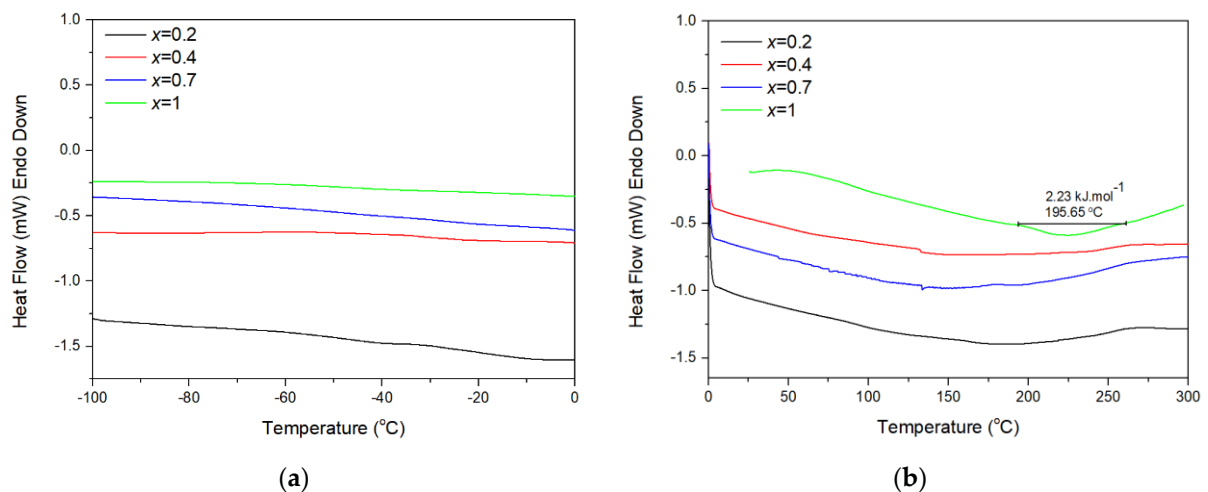


Figure 5. DSC curves for the $x = 0.2, 0.4, 0.7$ and 1 compositions in the family of $\text{Al}_{2-x}\text{In}_x\text{W}_3\text{O}_{12}$ at different temperatures: (a) cryogenic temperatures; (b) ambient and high temperatures. For $x = 1$, the onset temperature of the monoclinic-to-orthorhombic phase transition and the enthalpy of phase transition are presented as well.

TGA curves (see Supporting Information, Figure S3) of all four phases revealed mass losses <1 mass% over the temperature range from RT to 950 °C, classifying these materials as non-hygroscopic.

The analyses of data acquired by XRPD, dilatometry and DSC strongly support the finding of the monoclinic structure ($P2_1/a$ space group) at RT for the $x = 1$ material, which transforms to being orthorhombic at ca. 200 °C. These findings are not in line with the observations from earlier reports [12–14]. The inconsistencies can mostly likely be attributed to erroneous interpretation and analysis of XRPD patterns at RT [13,14]. A similar inconsistency was reported by Truitt et al. [27] for $\text{Fe}_{1.5}\text{Y}_{0.5}\text{Mo}_3\text{O}_{12}$, for which the orthorhombic system had been previously assigned down to -170 °C [28].

In the present study, no phase transition to a monoclinic (or other) phase was identified for $x = 0.2$, $x = 0.4$ or $x = 0.7$ over the temperature range of -100 °C to 300 °C (Figures 4 and 5). This feature of $\text{Al}_{2-x}\text{In}_x\text{W}_3\text{O}_{12}$ does not follow the electronegativity rule [4], contrary to the majority of $A_2M_3O_{12}$ materials [1,29]. By this rule, phase transition temperatures for the intermediate phases in the $\text{Al}_{2-x}\text{In}_x\text{W}_3\text{O}_{12}$ system would have values between the phase transition temperatures of the end members, i.e., between -22 °C and 250 °C. Other notable exemptions from the electronegativity rule are $\text{AlScMo}_3\text{O}_{12}$ [27] and the $\text{Al}_{2-x}\text{Sc}_x\text{W}_3\text{O}_{12}$ system [30,31]. Truitt et al. [27] proposed that a large difference in radii of the cations occupying octahedral position in $\text{AlScMo}_3\text{O}_{12}$ (Al/Sc ratio = 0.72) could contribute to such a finding. This difference is even higher for Al/In (ratio 0.675) and might explain the suppression of the transition to the monoclinic form in $x = 0.2$, $x = 0.4$ and $x = 0.7$ materials, but is not in the line with the observed phase transition for $\text{AlInW}_3\text{O}_{12}$ (at ~ 200 °C), which does fit the electronegativity rule. The unusual suppression of the orthorhombic-to-monoclinic transition in the present results for $\text{Al}_{2-x}\text{In}_x\text{W}_3\text{O}_{12}$ ($x = 0.2, 0.4$ and 0.7) and in a few other systems, namely $\text{AlScMo}_3\text{O}_{12}$ [27] and $\text{Al}_{2-x}\text{Sc}_x\text{W}_3\text{O}_{12}$ [30,31], still does not have a satisfactory explanation.

Intrinsic CTEs of the $x = 0.2$ and $x = 0.4$ phases are between the values of the end members, while the linear CTE for $x = 0.7$ is higher than for the $\text{In}_2\text{W}_3\text{O}_{12}$ end member [9]. This behavior of CTEs has been observed in related materials [29,32]. It is also relevant to note that the linear CTE of $\text{In}_2\text{W}_3\text{O}_{12}$ is positive [9] and very different from the negative linear CTE reported for its molybdate counterpart, $\text{In}_2\text{Mo}_3\text{O}_{12}$ [23]. Linear CTEs of $A_2M_3O_{12}$ phases were initially correlated with the cationic radii of A^{3+} , but now the octahedra volume distortion model [2,3] is considered to be more accurate and grounded in explaining the behavior of the linear CTE. The linear CTE of $\text{In}_2\text{W}_3\text{O}_{12}$ does not fit with cationic radii rationalization and is yet to be assessed in terms of the octahedra volume distortion model; however, it is confirmed by our results (Table 1 and Supporting Information, Table S1) that the $x = 0.2, 0.4$ and 0.7 materials in the $\text{Al}_{2-x}\text{In}_x\text{W}_3\text{O}_{12}$ family have low positive thermal expansion, as is the case for $\text{In}_2\text{W}_3\text{O}_{12}$.

On the other hand, orthorhombic $\text{AlInW}_3\text{O}_{12}$ showed a near-zero thermal expansion above 250 °C, in contrast with the other three compositions ($x = 0.2, 0.4$ and 0.7). This peculiar behavior of $\text{AlInW}_3\text{O}_{12}$ was also noted in the phase transition, since $x = 1$ was the only composition exhibiting a phase transition to the monoclinic form in accordance with the electronegativity rule.

4. Conclusions

This study showed that the $\text{Al}_{2-x}\text{In}_x\text{W}_3\text{O}_{12}$ system is not promising for designing materials with near-zero thermal expansion over a wide range that includes RT.

In contrast with some previous reports, this study provided solid proof that $\text{AlInW}_3\text{O}_{12}$ is monoclinic at RT and transforms to the orthorhombic form at ca. 200 °C. In addition, there was no evidence of orthorhombic-to-monoclinic phase transitions for $x = 0.2$, $x = 0.4$ and $x = 0.7$ materials in the $\text{Al}_{2-x}\text{In}_x\text{W}_3\text{O}_{12}$ family in the temperature interval from -100 °C to 500 °C.

Linear intrinsic CTEs of $x = 0.2$, $x = 0.4$ and $x = 0.7$ are low and positive between RT and 400 °C (ranging from 1.88×10^{-6} to 3.88×10^{-6} K^{-1}), and higher than the linear intrinsic CTE of the $\text{Al}_2\text{W}_3\text{O}_{12}$ end member in the $\text{Al}_{2-x}\text{In}_x\text{W}_3\text{O}_{12}$ series.

The suppression of the orthorhombic-to-monoclinic phase transition in $x = 0.2$, $x = 0.4$ and $x = 0.7$ materials does not align with expectations based on the electronegativity

rule. This finding, along with other literature reports, indicates that there are likely other mechanisms governing the orthorhombic-to-monoclinic phase transition in addition to the electronegativity of A^{3+} in octahedral sites.

Supplementary Materials: The following are available online at <https://www.mdpi.com/article/10.3390/ma14144021/s1>, Figure S1: HT-XRPD patterns of (a) $x = 0.2$; (b) $x = 0.4$; (c) $x = 0.7$ and (d) $x = 1$ phase, from RT to 400 °C, Figure S2-1: Natural logarithmic variations of unit-cell parameters (a, b and c) and unit-cell volume vs. temperature for $x = 0.2$ phase. (d), Figure S2-2: Natural logarithmic variations of unit-cell parameters (a, b and c) and unit-cell volume vs. temperature for $x = 0.4$ phase (d). Figure S2-3: Natural logarithmic variations of unit-cell parameters (a, b and c) and unit-cell volume vs. temperature for $x = 0.7$ phase (d), Figure S2-4: Natural logarithmic variations of unit-cell parameters (a, b and c) and unit-cell volume vs. temperature for $x = 1$ phase (monoclinic form) (d), Figure S2-5: Natural logarithmic variations of unit-cell parameters (a, b and c) and unit-cell volume vs. temperature for $x = 1$ phase (orthorhombic form) (d), Figure S3: TGA curves of phases in $Al_{2-x}In_xW_3O_{12}$ system: (a) $x = 0.2$; (b) $x = 0.4$; (c) $x = 0.7$ and (d) $x = 1$. Table S1: Theoretical, real and relative densities of $Al_{2-x}In_xW_3O_{12}$ phases with the nominal chemical compositions $x = 0.2$; $x = 0.4$; $x = 0.7$ and $x = 1$, Table S2: Unit-cell parameters at RT in $Al_{2-x}In_xW_3O_{12}$ system.

Author Contributions: Conceptualization, B.A.M.; Synthesis and overall characterizations, A.E.C.C.; Funding acquisition, B.A.M.; Methodology, A.E.C.C., A.D., M.B.J., M.A.W. and B.A.M.; Data interpretation, A.E.C.C., A.D., V.L.B., M.B.J., M.A.W. and B.A.M.; Writing—original draft, B.A.M.; Writing—review & editing, A.E.C.C., A.D., V.L.B., M.A.W. and B.A.M. All authors have read and agreed to the published version of the manuscript.

Funding: This study was financed in part by the Coordenação de Aperfeiçoamento de Pessoal de Nível Superior-Brasil (CAPES), finance code 001, by the U.S. Army Research Laboratory under the contract W911NF2020200; and by NSERC (Canada) under grant number RGPIN-2015-04593. A.E.C.C. is grateful to CNPq (National Council for Scientific and Technological Development) for a master's degree scholarship. B.A.M. is grateful to CNPq (National Council for Scientific and Technological Development) for a Research Productivity Grant.

Institutional Review Board Statement: Not applicable.

Informed Consent Statement: Not applicable.

Data Availability Statement: The data underlying this article will be shared on reasonable request from the corresponding author.

Acknowledgments: We acknowledge support from Dalhousie University through the Clean Technology Research Institute. A.E.C.C., A.D. and B.A.M. acknowledge support from FAPERJ, through the project E_12/2019.

Conflicts of Interest: The authors declare no conflict of interest. The funders had no role in the design of the study; in the collection, analyses, or interpretation of data; in the writing of the manuscript, or in the decision to publish the results.

References

1. Liu, H.; Sun, W.; Zhang, Z.; Lovings, L.; Lind, C. Thermal Expansion Behavior in the $A_2M_3O_{12}$ Family of Materials. *Solids* **2021**, *2*, 87–107. [[CrossRef](#)]
2. Marinkovic, B.A.; Ari, M.; de Avillez, R.; Rizzo, F.; Ferreira, F.F.; Miller, K.J.; Johnson, M.B.; White, M.A. Correlation between AO_6 Polyhedral Distortion and Negative Thermal Expansion in Orthorhombic $Y_2Mo_3O_{12}$ and Related Materials. *Chem. Mater.* **2009**, *21*, 2886–2894. [[CrossRef](#)]
3. Romao, C.P.; Perras, F.A.; Werner-Zwanziger, U.; Lussier, J.A.; Miller, K.J.; Calahoo, C.M.; Zwanziger, J.W.; Bieringer, M.; Marinkovic, B.A.; Bryce, D.L.; et al. Zero Thermal Expansion in $ZrMgMo_3O_{12}$: NMR Crystallography Reveals Origins of Thermoelastic Properties. *Chem. Mater.* **2015**, *27*, 2633–2646. [[CrossRef](#)]
4. Sleight, A.; Brixner, L. A new ferroelastic transition in some $A_2(MO_4)_3$ molybdates and tungstates. *J. Solid State Chem.* **1973**, *7*, 172–174. [[CrossRef](#)]
5. Woodcock, D.A.; Lightfoot, P.; Ritterb, C. Negative Thermal Expansion in $Y_2(WO_4)_3$. *J. Solid State Chem.* **2000**, *149*, 92–98. [[CrossRef](#)]
6. Imanaka, N.; Hiraiwa, M.; Adachi, G.; Dabkowska, H.; Dabkowski, A. Thermal contraction behavior in $Al_2(WO_4)_3$ single crystal. *J. Cryst. Growth* **2000**, *220*, 176–179. [[CrossRef](#)]

7. Sivasubramanian, V.; Ravindran, T.R.; Nithya, R.; Arora, A.K. Structural phase transition in indium tungstate. *J. Appl. Phys.* **2004**, *96*, 387–392. [[CrossRef](#)]
8. Hashimoto, T.; Sugimoto, T.; Omoto, K.; Kineri, N.; Ogata, Y.; Tsuda, K. Analysis of phase transition and expansion behaviour of $\text{Al}_2(\text{WO}_4)_3$ by temperature-regulated X-ray diffraction. *Phys. Status Solidi B* **2008**, *245*, 2504–2508. [[CrossRef](#)]
9. Baiz, T.I.; Heinrich, C.P.; Banek, N.A.; Vivekens, B.L.; Lind, C. In-situ non-ambient X-ray diffraction studies of indium tungstate. *J. Solid State Chem.* **2012**, *187*, 195–199. [[CrossRef](#)]
10. Liu, H.; Zhang, Z.; Ma, J.; Jun, Z.; Zeng, X. Effect of isovalent substitution on phase transition and negative thermal expansion of $\text{In}_{2-x}\text{Sc}_x\text{W}_3\text{O}_{12}$ ceramics. *Ceram. Int.* **2015**, *41*, 9873–9877. [[CrossRef](#)]
11. Evans, J.; Mary, T.A. Sleight, Negative thermal expansion in a large molybdate and tungstate family. *J. Solid State Chem.* **1997**, *275*, 61–65. [[CrossRef](#)]
12. Mary, T.A.; Sleight, A.W. Bulk thermal expansion for tungstate and molybdates of the type $\text{A}_2\text{M}_3\text{O}_{12}$. *J. Mater. Res.* **1999**, *14*, 912–915. [[CrossRef](#)]
13. Tzvetkov, P.; Ivanova, D.; Kovacheva, D.; Nikolov, V. Synthesis and powder XRD characterization of $\text{Al}_{2-x}\text{In}_x(\text{WO}_4)_3$ solid solutions. *J. Alloy. Compd.* **2009**, *470*, 492–496. [[CrossRef](#)]
14. Zhecheva, E.; Stoyanova, R.; Ivanova, S.; Nikolov, V. On the preparation of nanosized $\text{Al}_2(\text{WO}_4)_3$ by a precipitation method. *Solid State Sci.* **2010**, *12*, 2010–2014. [[CrossRef](#)]
15. Yordanova, A.S.; Nikolov, V.S.; Koseva, I.I. Fabrication of high density ceramic from $\text{Al}_{2-x}\text{In}_x(\text{WO}_4)_3$ solid solutions. *J. Chem. Technol. Metall.* **2015**, *50*, 537–542.
16. Pontón, P.I.; Prisco, L.P.; Dosen, A.; Faro, G.S.; de Abreu, M.A.; Marinkovic, B.A. Co-precipitation synthesis of $\text{Y}_2\text{W}_3\text{O}_{12}$ submicronic powder. *Ceram. Int.* **2017**, *43*, 4222–4228. [[CrossRef](#)]
17. Miller, K.J.; Johnson, M.B.; White, M.A.; Marinkovic, B.A. Low-temperature investigations of the open-framework material $\text{HfMgMo}_3\text{O}_{12}$. *Solid State Commun.* **2012**, *152*, 1748–1752. [[CrossRef](#)]
18. Costa, I.L.M.; Blair, V.L.; Paraguassu, W.; Marinkovic, B.A. Evaluating $\text{Al}_{2-x}\text{Ga}_x\text{W}_3\text{O}_{12}$ system for thermal shock resistance. *J. Solid State Chem.* **2019**, *277*, 149–158. [[CrossRef](#)]
19. Sugimoto, Y.; Aoki, T.; Niwa, Y.; Hashimoto, E.; Morito, T. Thermal Expansion and Phase Transition Behavior of $\text{Al}_{2-x}\text{M}_x(\text{WO}_4)_3$ ($\text{M} = \text{Y}, \text{Ga}$ and Sc) Ceramics. *J. Ceram. Soc. Jap.* **2007**, *115*, 176–181. [[CrossRef](#)]
20. Jacob, K.T.; Raj, S.; Rannesh, L. Vegard's law: A fundamental relation or an approximation? *Int. J. Mater. Res.* **2007**, *98*, 776–779. [[CrossRef](#)]
21. Shannon, R.D. Revised effective ionic radii and systematic studies of interatomic distances in halides and chalcogenides. *J. Acta Crystallogr. A* **1976**, *32*, 751–767. [[CrossRef](#)]
22. Evans, J.; Mary, T. Structural phase transitions and negative thermal expansion in $\text{Sc}_2(\text{MoO}_4)_3$. *Int. J. Inorg. Mater.* **2000**, *2*, 143–151. [[CrossRef](#)]
23. Marinkovic, B.A.; Ari, M.; Jardim, P.; de Avillez, R.R.; Rizzo, F.; Ferreira, F.F. $\text{In}_2\text{Mo}_3\text{O}_{12}$: A low negative thermal expansion compound. *Thermochim. Acta* **2010**, *499*, 48–53. [[CrossRef](#)]
24. Romao, C.P.; Donegan, S.P.; Zwanziger, J.W.; White, M.A. Relationships between elastic anisotropy and thermal expansion in $\text{A}_2\text{M}_3\text{O}_{12}$ materials. *Phys. Chem. Chem. Phys.* **2016**, *18*, 30652–30661. [[CrossRef](#)] [[PubMed](#)]
25. Prisco, L.P.; Pontón, P.; Paraguassu, W.; Romao, C.; White, M.A.; Marinkovic, B.A. Near-zero thermal expansion and phase transition in $\text{In}_{0.5}(\text{ZrMg})_{0.75}\text{Mo}_3\text{O}_{12}$. *J. Mater. Res.* **2016**, *31*, 3240–3248. [[CrossRef](#)]
26. Varga, T.; Moats, J.L.; Ushakov, S.; Navrotsky, A. Thermochemistry of $\text{A}_2\text{M}_3\text{O}_{12}$ negative thermal expansion materials. *J. Mater. Res.* **2007**, *22*, 2512–2521. [[CrossRef](#)]
27. Truitt, R.; Hermes, I.; Main, A.; Sendekci, A.; Lind, C. Low Temperature Synthesis and Characterization of $\text{AlScMo}_3\text{O}_{12}$. *Materials* **2015**, *8*, 700–716. [[CrossRef](#)]
28. Li, Z.Y.; Song, W.B.; Liang, E.J. Structures, Phase Transition, and Crystal Water of $\text{Fe}_{2-x}\text{Y}_x\text{Mo}_3\text{O}_{12}$. *J. Phys. Chem. C* **2011**, *115*, 17806–17811. [[CrossRef](#)]
29. Ari, M.; Jardim, P.; Marinkovic, B.; Rizzo, F.; Ferreira, F.F. Thermal expansion of $\text{Cr}_{2x}\text{Fe}_{2-2x}\text{Mo}_3\text{O}_{12}$, $\text{Al}_{2x}\text{Fe}_{2-2x}\text{Mo}_3\text{O}_{12}$ and $\text{Al}_{2x}\text{Cr}_{2-2x}\text{Mo}_3\text{O}_{12}$ solid solutions. *J. Solid State Chem.* **2008**, *181*, 1472–1479. [[CrossRef](#)]
30. Zhu, J.; Yang, J.; Cheng, X. Synthesis and tunable thermal expansion property of $\text{Al}_{2-\delta}\text{Sc}_\delta\text{W}_3\text{O}_{12}$. *Solid State Sci.* **2012**, *14*, 187–190. [[CrossRef](#)]
31. Dasgupta, N.; Sorge, E.; Butler, B.; Wen, T.-C.; Shetty, D.K.; Cambrea, L.R.; Harris, D.C. Synthesis and characterization of $\text{Al}_{2-x}\text{Sc}_x(\text{WO}_4)_3$ ceramics for low-expansion infrared-transmitting windows. *J. Mater. Sci.* **2012**, *47*, 6286–6296. [[CrossRef](#)]
32. Liu, J.; Maynard-Casely, H.E.; Brand, H.E.A.; Sharma, N. $\text{Sc}_{1.5}\text{Al}_{0.5}\text{W}_3\text{O}_{12}$ Exhibits Zero Thermal Expansion between 4 and 1400 K. *Chem. Mater.* **2021**, *33*, 3823–3831. [[CrossRef](#)]